— EPAPS Supplementary online material —
Evidence of precursor superconductivity as high as 180 K from infrared spectroscopy

A. Dubroka,[1] M. Rössle,[1] K.W. Kim,[1] V.K. Malik,[1] D. Munzar,[2] D.N. Basov,[3] A. Schafgans,[3] S.J. Moon,[3] C.T. Lin,[4] D. Haug,[4] V. Hinkov,[4] B. Keimer,[4] Th. Wolf,[5] J.G. Storey,[6] J.L. Tallon,[6] and C. Bernhard[1]

[1] *Department of Physics and Fribourg Center for Nanomaterials, University of Fribourg, Chemin du Musee 3, 1700 Fribourg, Switzerland.*
[2] *Department of Condensed Matter Physics, Faculty of Science, Masaryk University, Kotlářská 2, 61137 Brno, Czech Republic.*
[3] *Department of Physics, University of California, San Diego, La Jolla, California 92093, USA.*
[4] *Max-Planck-Institut für Festkörperforschung, Heisenbergstrasse 1, D-70569 Stuttgart, Germany.*
[5] *Karlsruhe Institute of Technology, D-76021 Karlsruhe, Germany.*
[6] *MacDiarmid Institute, Industrial Research Ltd., P.O. Box 31310, Lower Hutt, New Zealand.*

I. ANALYSIS OF THE *c*-AXIS RESPONSE

A. Parameterization of the *c*-axis spectra

The frequency and the broadening of the phonon lineshape, as displayed in Fig. 2(a) and 2(b) of the paper, have been obtained by fitting the real and imaginary parts of the measured spectra with the following function:

$$\epsilon(\omega) = \epsilon_\infty + \sum_j \frac{\omega_{\mathrm{p},j}^2 - \mathrm{i}\omega\beta_j}{\omega_{0,j}^2 - \omega^2 - \mathrm{i}\omega\gamma_j} \,. \qquad (1)$$

The sum consists of Lorentzian functions with a complex oscillator strength [1]. The imaginary part of the oscillator strength $\mathrm{i}\omega\beta_j$ enables us to describe the lineshapes of phonons even if they are renormalized by an interaction, for example, with other phonons or the electronic background. Note that this formula satisfies the condition of Kramers-Kronig consistency $\epsilon(-\omega) = \epsilon(\omega)^*$. It allows us to obtain very good fits (within the noise level of the experimental data) with only one oscillator per an IR-active phonon mode and a few broad resonances for the electronic background. We do not assign any physical significance to the obtained values of the parameters but merely use them to reliably identify the anomalies in the temperature dependence of the phonon modes, as shown in Figs. 1(c) and 2(a-b) of the paper.

B. The multilayer model

In the paper, we analyzed our data with a model that describes the electromagnetic response of a stack of superconducting layers that are separated by different kinds of spacer layers through which they are weakly coupled along the *c*-axis direction. This so-called multilayer model [2–4] has been shown to reproduce very well the *c*-axis response of the bilayer compounds like $YBa_2Cu_3O_{7-\delta}$ where the conductivity between the closely-spaced CuO_2 layers (intra-bilayer region, "bl") is substantially different (higher) from the one between the bilayers (inter-bilayer region, "int"). For this geometry, which essentially corresponds to two resistors in series, there exists a frequency at which the charge density resonantly oscillates between the CuO_2 planes of the bilayers. This oscillation forms an electric dipole and thus is infrared active and shows up as an absorption band in the spectra, the so called transverse plasma mode (TPM). Munzar *et al.* [4, 5] successfully explained the interaction of the TPM with the IR-active phonons and the resulting phonon anomalies, in particular the one of the phonon at $320\,\mathrm{cm}^{-1}$. They showed that the renormalization of the phonons naturally results from the superconductivity induced changes of the charge density oscillations.

For our analysis we used the same structure of the interaction between the phonons and the electronic degrees of freedom as introduced in Ref. [4]. The electronic background is expressed in terms of the intra-bilayer and inter-bilayer current densities, j_{bl} and j_{int}, respectively, which are related to the corresponding local fields E_{bl} and E_{int} and the local susceptibilities χ_{bl} and χ_{int}, as

$$j_{\mathrm{bl}}(\omega) = -\mathrm{i}\omega\epsilon_0\chi_{\mathrm{bl}}(\omega)E_{\mathrm{bl}}(\omega) \,, \qquad (2)$$
$$j_{\mathrm{int}}(\omega) = -\mathrm{i}\omega\epsilon_0\chi_{\mathrm{int}}(\omega)E_{\mathrm{int}}(\omega) \,. \qquad (3)$$

The susceptibilities $\chi_{\mathrm{bl}}(\omega)$ and $\chi_{\mathrm{int}}(\omega)$ are modeled by the following set of Drude-Lorentz oscillators

$$\chi_a(\omega) = -\frac{\omega_a^2}{\omega^2} - \frac{\Omega_a^2}{\omega(\omega + \mathrm{i}\gamma_a)} + \\ + \sum_j \frac{S_{a,j}^2}{\nu_{a,j}^2 - \omega^2 - \mathrm{i}\omega\Gamma_{a,j}} \,, \quad a \in \{\mathrm{bl}, \mathrm{int}\} \,. \qquad (4)$$

The first and the second term account for the response of the superconducting condensate and the quasiparticles with finite scattering rate (Drude term), respectively. We find that the broadening of the Drude term γ_{bl} of the intra-bilayer response above T_c is about $150\,\mathrm{cm}^{-1}$ and remains nearly temperature independent. In order to reduce the number of free parameters, we have fixed γ_{bl} at this value for all temperatures. An alternative modeling approach where γ_{bl} is fitted at every temperature independentely is discussed below. The spectral weight of the Drude term, $\mathrm{SW}_{\mathrm{bl}}^{\mathrm{Drude}} = \Omega_{\mathrm{bl}}^2$, was fitted and its temperature dependence is shown in Fig. 1(f) of the paper. In the

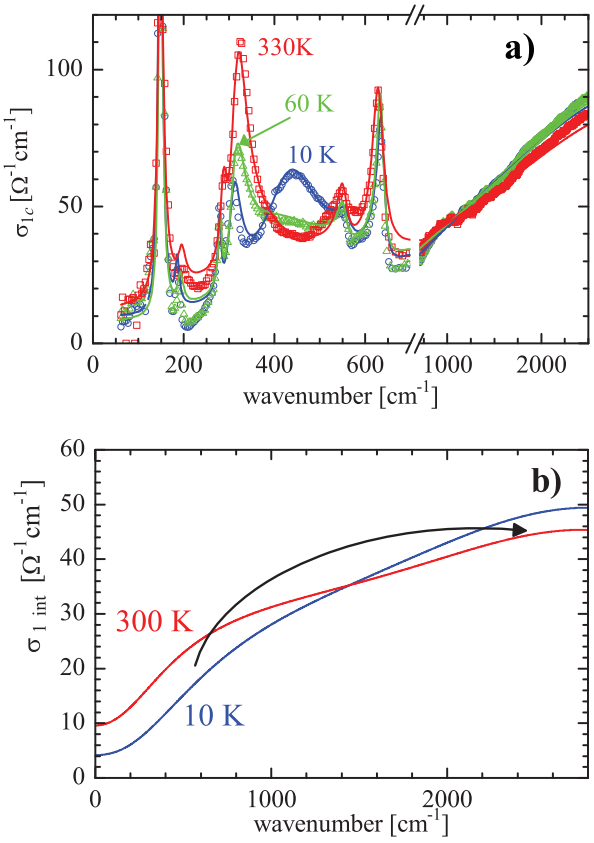

Fig. S 1: a) The data and fit with the MLM from the paper Fig. 1 a) shown on a broader frequency range. b) The real part of the inter-bilayer conductivity $\sigma_{1,\mathrm{int}}$ showing the upwards shift of the spectral weight due to the extrinsic pseudogap below T^*.

spectra below T_c, the weight of this Drude term is transferred to the one of the SC term $\mathrm{SW}_{\mathrm{bl}}^{\mathrm{SC}} = \omega_{\mathrm{bl}}^2$ as shown in Fig. 1(f) of the paper. We note that in the intra-bilayer conductivity, σ_{bl}, our fit cannot distinguish between a superconducting delta function at the origin and a Drude term with a very small damping ($\gamma_{\mathrm{bl}} < 30\,\mathrm{cm}^{-1}$).

The sum in Eq. (4) represents the additional oscillators that were necessary to fit the higher energy part of the spectra above $1000\,\mathrm{cm}^{-1}$. Since the response is only slowly varying, two broad oscillators located at about 1500 and $3000\,\mathrm{cm}^{-1}$ were sufficient. These oscillators are almost temperature independent in the case of the intra-bilayer response. In contrast, in the inter-bilayer response they significantly change with temperature and track the decrease of the low frequency spectral weight related to the competing pseudogap as shown in Fig. 1(d) of the paper. Supplementary Fig. 1a) shows the data and fit on a broader frequency scale and Fig. 1b) the resulting inter-bilayer conductivity that demonstrates that the missing low frequency spectral weight is shifted to higher frequencies. This trend originates from the similar feature of the broad background in the raw data shown in Fig. 1a) or in Fig. 1(b) of the paper.

As was outlined previously [4], the phonons at 280, 560 and $620\,\mathrm{cm}^{-1}$ involve predominantly vibrations of the oxygen ions in the inter-bilayer region whereas the $320\,\mathrm{cm}^{-1}$ phonon is due to the bond-bending vibration of the oxygen ions in the CuO_2 planes. The coupling between these phonons, the local fields E_{bl} and E_{int}, and the inter- and intra-bilayer current densities is described in detail in Ref. [5]. Here we focus on the $320\,\mathrm{cm}^{-1}$ phonon and its anomalous temperature dependence which is playing a central role in the analysis as presented in the paper. We emphasize that the values of the bare oscillator strength and bare frequency of this phonon were determined from the room temperature spectra and then kept fixed for all the fits to the spectra of lower temperatures. The large and anomalous changes of the parameters (oscillator strength, frequency, and broadening) of the lineshape this phonon mode therefore arise from the coupling to the inter- and intra-bilayer current densities and the changes of these quantities with temperature. For the fitting, we simultaneously used the real- and imaginary parts of the optical conductivity which were determined independently by ellipsometry.

We note that the temperature dependence of the intra-bilayer current density, σ_{bl}, affects the optical spectra mainly below $700\,\mathrm{cm}^{-1}$ where the phonon anomalies and the TPM occur. On the other hand, the inter-bilayer response, σ_{int}, exhibits temperature dependent changes of the broad electronic background where the conductivity is reduced at lower frequency and the spectral weight is shifted to frequencies above $1000\,\mathrm{cm}^{-1}$ as the competing pseudogap develops below T^*. Therefore, the two kinds of inter- and intra-bilayer current densities give rise to clearly distinct spectroscopic features whose determination is well conditioned.

In the following we show that a qualitatively similar result is obtained, concerning the increase of the coherent low-frequency spectral weight in $\sigma_{1,\mathrm{bl}}$ below T^{ons}, even if we do not fix the value of γ_{bl}. In this case, we do not need to include an additional delta function at $\omega = 0$ below T_c since it can be hardly distinguished from the Drude term which also gets very narrow with $\gamma_{\mathrm{bl}} < 10\,\mathrm{cm}^{-1}$ at $T << T_c$. All the spectral weight of the coherent low frequency response is thus contained in the Drude term, i.e. in $\mathrm{SW}_{\mathrm{bl}}^{\mathrm{Drude}} = \Omega_{\mathbf{bl}}^2$. Supplementary Fig. 2(a) shows that this modified MLM model also provides a good description of the experimental data and supplementary Figs. 2(b) and 2(c) confirm that the obtained spectra of $\sigma_{1,\mathrm{bl}}$ exhibit a similar trend as it was presented above where we fixed γ_{bl} to $150\,\mathrm{cm}^{-1}$. In particular, the spectral weight of the Drude response is essentially constant above $T^{\mathrm{ons}} \approx 160$ K, while it exhibits a clear increase below T^{ons}. This increase is even more pronounced here since in parallel the value of γ_{bl} also increases slightly below T^{ons}. As such it can be concluded that the model with a fixed broadening of the Drude term, as presented in Figure 1 of the paper, provides

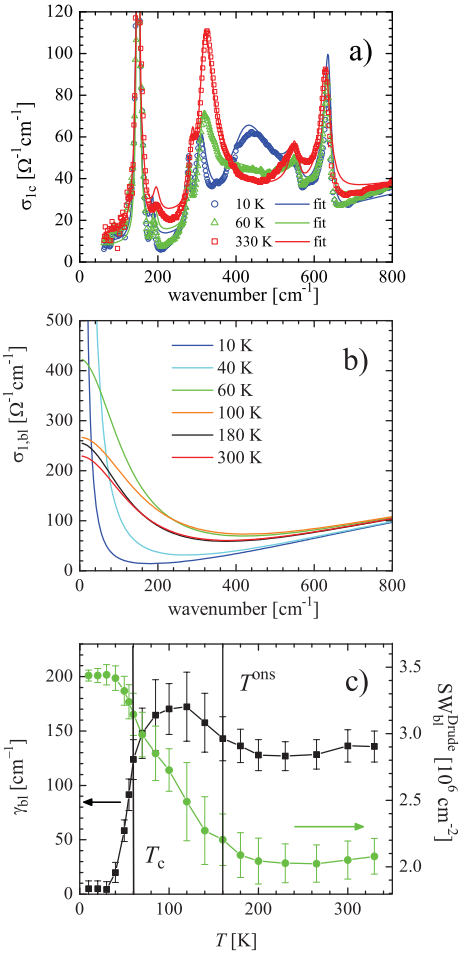

Fig. S 2: **a,** Comparison of the measured spectra of the c-axis conductivity of underdoped Y-123 with $T_c = 58$ K and the fits with the MLM where the width of the Drude term in $\sigma_{1,bl}$ has not been fixed. **b,** The obtained spectra of the intra-bilayer conductivity, $\sigma_{1,bl}$. **c**, Temperature dependence of the spectral weight, SW_{bl}^{Drude}, and the width, γ_{bl}, of the Drude term.

a lower limit for the increase of the coherent spectral weight below $T^{ons} \approx 160$ K. Finally, below T_c the value of γ_{bl} decreases sharply and almost vanishes at $T << T_c$ thus confirming that the vast majority of the low-energy intra-bilayer spectral weight participates in the superconducting condensate.

C. Doping dependence of the far-infrared c-axis conductivity

Supplementary Fig. 3(a-e) displays the spectra of the far-infrared c-axis conductivity of a series of Y-123 single crystals whose doping level decreases successively from optimally doped (a), to strongly underdoped (e). The graphs show representative spectra well above T^{ons} (red line), near T^{ons} (black line), at T_c (green line), and at 10 K (blue). For the near optimally doped sample Y-123 with $T_c = 90$ K [see supplementary Fig. 3(a)] the spectra show no evidence of any anomalous features above $T_c = 90$ K, i.e. the spectrum at 140 K almost overlaps with the one at 90 K. This is already very different for the moderately underdoped sample with $T_c = 75$ K, as shown in supplementary Fig. 3(b). The pseudogap below $T^* = 260$ K gives rise to a clear suppression of the elec-

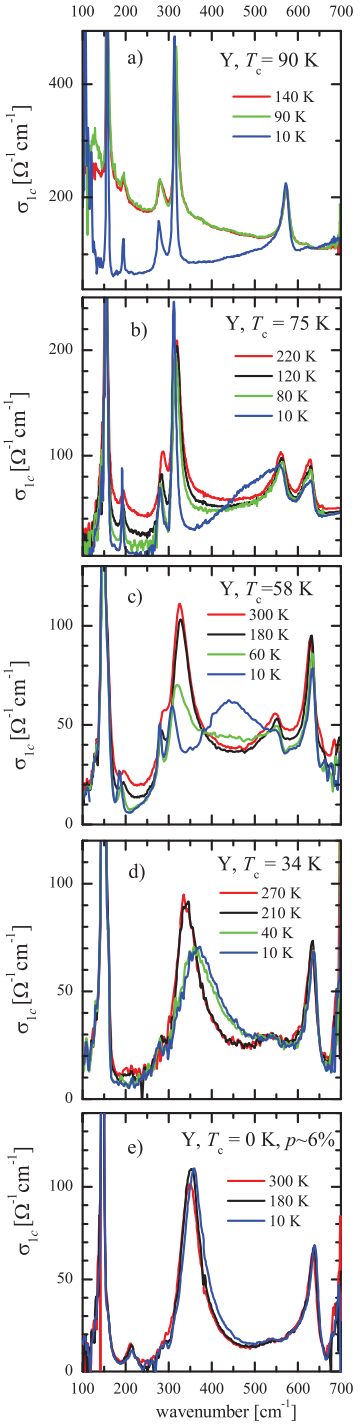

Fig. S 3: **a-e**, The c-axis conductivity of samples with doping gradually decreasing from optimally doped one (a), to extremely underdoped one (e).

tronic conductivity, i.e. the broad electronic background of the spectrum at 120 K is already significantly lower than the one at 220 K. In comparison, the features related to $T^{\rm ons} = 120$ K are still fairly weak and difficult to identify from the inspection of the spectra. Nevertheless, the softening of the $320\,{\rm cm}^{-1}$ phonon mode is obvious from the fits of the data as shown in Fig. 1 of the paper. The same applies to the TPM which becomes most pronounced below $T_{\rm c}$ (blue line) where it gives rise to a band around $500\,{\rm cm}^{-1}$.

In the strongly underdoped sample Y-123 with $T_{\rm c} = 58$ K [see supplementary Fig. 3(c)], the effects related to $T^{\rm ons} = 160$ K are already very pronounced. One can see that the spectral weight of the lineshape of the $320\,{\rm cm}^{-1}$ phonon is substantially reduced and the frequency is softened when going from 180 K (black) to $T_{\rm c}$=60 K (green). The same applies for the TPM at $450\,{\rm cm}^{-1}$ which is already noticeable at 60 K. In the very underdoped sample Y-123 with $T_{\rm c} = 34$ K [see supplementary Fig. 3(d)] the competing pseudogap is already fully developed above 300 K, therefore there is hardly any difference between the spectra at 270 K and 210 K. Nevertheless, the spectrum at 40 K right above $T_{\rm c}$ (green) differs drastically from the one at 210 K (black). The TPM merges here with the phonon at $320\,{\rm cm}^{-1}$. Below $T^{\rm ons} \approx 180$ K, the phonon-TPM band broadens dramatically and is shifted to higher frequencies. The main effect occurs here above $T_{\rm c}$, while only a slight additional increase of the frequency occurs below $T_{\rm c}$.

Note that the magnitude of the changes associated with the TPM and the phonon anomalies at $T_{\rm c} < T < T^{\rm ons}$ becomes relatively large in the strongly underdoped regime. While in the sample with $T_{\rm c} = 58$ K the changes have about the same magnitude or are smaller than the ones below $T_{\rm c}$ this is reversed for the sample with $T_{\rm c} = 34$ K where the largest changes already occur between $T^{\rm ons}$ and $T_{\rm c}$. With decreasing doping, the effects related to $T^{\rm ons}$ become stronger while the ones below $T_{\rm c}$ become relatively much weaker. Notably similar relation between the magnitude of the changes below $T^{\rm ons}$ and below $T_{\rm c}$ has been observed in independent experiments, like the Nernst effect [7], dilatometry [8], specific heat [9, 10] and can also be noticed from the temperature evolution of the intensity of the magnetic resonance mode in inelastic neutron scattering measurements [11, 12]. Finally, even for the sample Y-123 with $T_{\rm c} = 0$ K and $p \approx 6\%$ [see supplementary Fig. 3(e)], we still observe a noticeable increase of the frequency and broadening of the phonon-TPM band between 180 K and 10 K.

D. Bilayer splitting and the c-axis hopping matrix elements

In bilayer cuprate superconductors like Y-123, the conduction band of the copper-oxygen planes is split into bonding band (B) and antibonding band (A), respectively. Their dispersions are conveniently parameterized as

$$\epsilon_{B/A}(\mathbf{k}_\parallel, k_z) = \epsilon(\mathbf{k}_\parallel) \mp \sqrt{t^2_{\perp\,\rm bl}(\mathbf{k}_\parallel) + t^2_{\perp\,\rm int}(\mathbf{k}_\parallel) + 2t_{\perp\,\rm bl}(\mathbf{k}_\parallel) t_{\perp\,\rm int}(\mathbf{k}_\parallel) \cos(k_z d)}\,. \tag{5}$$

Here ϵ is the in-plane component, that can be expressed in terms of hopping matrix elements between orbitals of a single plane. The parameters $t_{\perp\,\rm bl}$ and $t_{\perp\,\rm int}$ are the $\mathbf{k}_\parallel$-dependent hopping matrix elements between the closely-spaced planes and the widely-spaced planes, respectively, that can be expressed in terms of hopping matrix elements between orbitals of different planes. The magnitude of $t_{\perp\,\rm bl}$ is much higher than that of $t_{\perp\,\rm int}$. It follows from Eq. (5) that the splitting of the conduction band is approximately equal to $2t_{\perp\,\rm bl}$:

$$\Delta\epsilon = \epsilon_A - \epsilon_B \approx 2t_{\perp\,\rm bl}\,. \tag{6}$$

According to the analysis by O. Andersen and coworkers [13], the inter-plane hopping proceeds mainly through the copper 4s orbitals. Considerations of this hopping channel yield [13]

$$t_{\perp\,\rm int/bl} \approx \frac{t_{\perp\,\rm int/bl}(X)}{4}\left[\cos(k_x a) - \cos(k_y a)\right]^2\,, \tag{7}$$

where X stands for $(\pi/a, 0)$ and a is the lattice parameter. The inter-bilayer hopping in Y-123 involves the apical oxygen $2p_z$ orbitals, that can be accessed from the copper 4s only. This suggests that Eq. (7) provides a realistic approximation to $t_{\perp\,\rm int}$. The hopping thus can be expected to attain its maximum at the X-point (in the so-called antinodal region where the extrinsic pseudogap prevails) to vanish along the BZ diagonal and to be small around the diagonal, in the so called nodal region, where well-defined quasiparticles persist even in strongly underdoped samples. The calculated $\mathbf{k}_\parallel$-dependence of $t_{\perp\,\rm bl}$ (see Fig. 7 (b) of Ref. [13]) exhibits a maximum close to the X-point, consistent with the considerations of the copper 4s channel, but the magnitude of $t_{\perp\,\rm bl}$ at the BZ diagonal is only by a factor of about 2 smaller than that at the X-point. Photoemission experiments on Y-123 [14, 15] suggest an even weaker anisotropy of the effective intra-bilayer hopping which, consistent with Eq. (6), is defined as one half of the bilayer splitting.

E. Formulas for the local conductivities

Starting from a perturbative treatment of the c-axis coupling, one arrives at the following equations for the

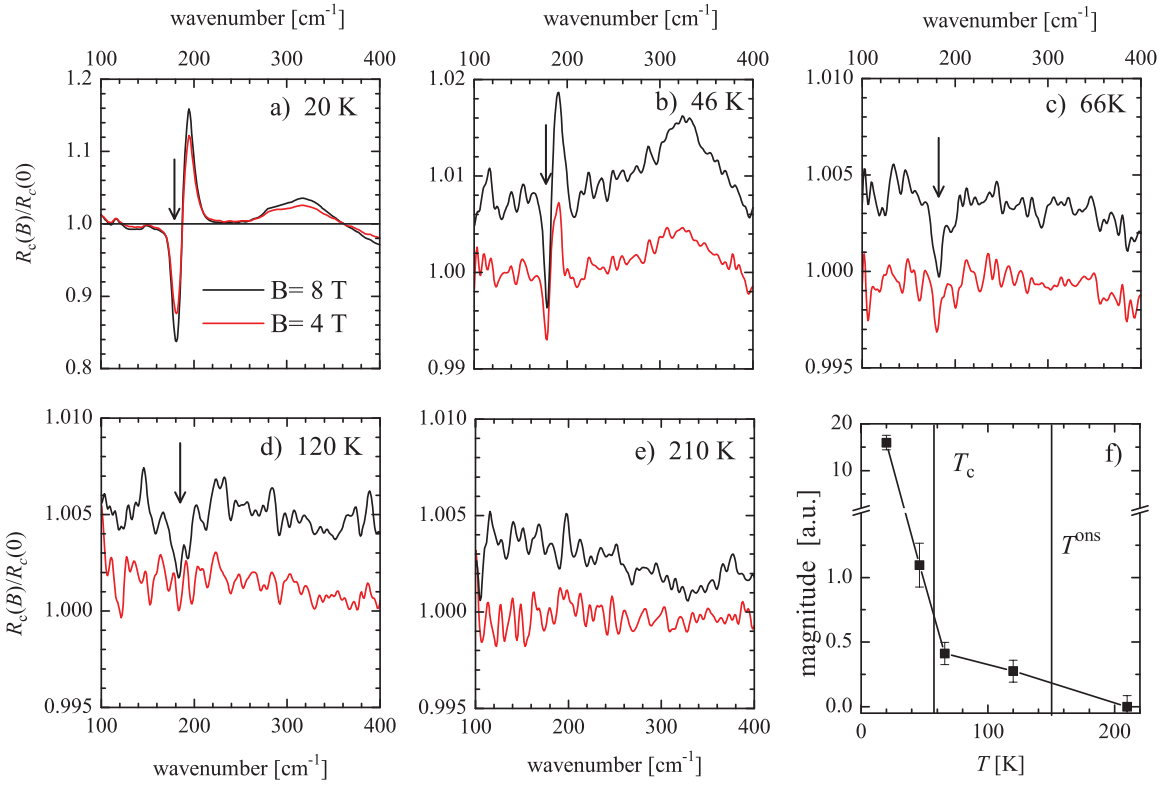

Fig. S 4: Magnetic field dependence of the c-axis response of an underdoped Y-123 sample with $T_c = 56$ K. **a-e**, Spectra of the c-axis reflectivity in the magnetic field parallel to the c-axis, $R_c(B)$; shown is the ratio with respect to the spectrum at zero field. The spectra at 8 T at $T \geq 46$ K have been shifted up for clarity. The feature at around 185 cm^{-1} is marked by the arrows. **f**, Temperature dependence of the magnitude of the 185 cm^{-1} feature.

real parts of the local conductivities [16, 17]:

$$\mathrm{Re}\,\sigma_{\mathrm{int/bl}}(\omega) = k\frac{d_{\mathrm{int/bl}}}{\omega}\sum_{\mathbf{k}_\parallel} t^2_{\perp\,\mathrm{int/bl}}(\mathbf{k}_\parallel)\cdot$$

$$\cdot\int d\omega' A(\mathbf{k}_\parallel,\omega+\omega')A(\mathbf{k}_\parallel,\omega')[n_F(\omega')-n_F(\omega+\omega')]\,, \tag{8}$$

where k is a constant, d_{int} and d_{bl} are the distances between the closely-spaced and the widely-spaced planes, respectively, $A(\mathbf{k}_\parallel,\omega)$ is the quasiparticle spectral function of the copper oxygen plane, and n_F the Fermi-Dirac function. For the sake of simplicity, we have limited ourselves to the normal state, an extension of Eq. (8) is needed to describe the response of the superconducting state. The fact that the conductivities are expressed in terms of the quasiparticle spectral function, allows one to correlate the c-axis infrared data with the ones from photoemission [18]. The Eqs. (8), together with the properties of the hopping matrix elements as described above and the well known dichotomy between the antinodal and the nodal region in the underdoped regime [19], provide a background for interpreting the difference between σ_{bl} and σ_{int} as obtained by fitting the data. Below T^{ons}, the difference is probably enhanced due to a partial phase coherence within the bilayer units as suggested in [4, 20].

The perturbative approach leading to Eq. (8) is justified if both $t_{\perp\,\mathrm{int}}$ and $t_{\perp\,\mathrm{bl}}$ are smaller than any relevant in-plane energy scale. For Y-123, the bare values of $t_{\perp\,\mathrm{bl}}$ are fairly large, of the order of 0.1 eV, and it is thus not obvious that σ_{bl} can be discussed using Eq. (8). Below we present arguments suggesting that in strongly underdoped Y-123 the bilayer splitting is drastically renormalized and the use of Eq. (8) is thus meaningful.

(a) Some of us have recently studied the c-axis response using a nonperturbative approach involving the bilayer split bands [21]. The calculated superconducting-state spectra of the real part of the conductivity display two superconductivity-induced features due to the presence of the bilayer unit:

(i) a collective mode T_1 at an energy given by a Brillouin zone average of $\Delta\epsilon$, somewhat blue-shifted by virtue of the Coulomb interaction and

(ii) a pair-breaking bonding-antibonding peak T_2 well above the superconducting gap 2Δ. The smaller the bilayer splitting the smaller the spectral weight of T_2.

Experimental spectra of moderately underdoped Y-123 also display two superconductivity induced features: the TPM, that is the subject of this study, and a maximum around 1000 cm^{-1} [22]. A detailed comparison between theoretical and experimental spectra provides the following assignment: T_1 belongs to the TPM and T_2 to the

maximum around 1000 cm^{-1}. With decreasing doping, the frequency of the TPM decreases dramatically, and for doping levels below ca 10 % the maximum around 1000 cm^{-1} vanishes (see supplementary Fig. 3 and Fig. 13 of Ref. [21]). These experimental results indicate that in strongly underdoped Y-123 with the hole doping around 10 % the effective intra-bilayer hopping is very small. The intra-bilayer conductivity can then be approximated by Eq. (8) (see the discussion of Fig. 15 in Ref. [21]).
(b) Results of photoemission experiments on Y-123 samples with the surface doping controlled through in situ deposition of potassium atoms reveal a collapse of the bonding and antibonding Fermi surfaces into four nodal Fermi arcs for doping levels below ca 10 % [23, 24], consistent with the findings based on infrared.

II. MAGNETO-OPTICAL MEASUREMENTS

The magneto-optical measurements were performed in a split-coil superconducting magnet. First, the power spectra of the sample in magnetic field were measured. The time stability of the measurement was ensured by normalizing the signal to the one of an in-situ stainless-steel reference mirror. Secondly, the sample was in situ coated with Au and the measurements in the magnetic field were repeated in order to subtract any instability of the setup with the change of the magnetic field. In such a way, it is possible to reduce the systematic errors in the $R(B)/R(B=0)$ ratio to the level of about 10^{-3}.

Supplementary Fig. 4 shows our magneto-optical spectra for a YBCO sample with $T_\mathrm{c} = 56\,\mathrm{K}$ and $T^\mathrm{ons} = 175\,\mathrm{K}$ which is a bit more strongly underdoped than the sample, whose spectra are presented in Fig. 3 of the paper. It shows that the magnetic-field-induced anomaly of the 185 cm^{-1} phonon mode (the dip marked by arrows) persists up to at least 120 K [see supplementary Figs. 4(a)-(d)] and is absent at 210 K [supplementary Fig. 4(e)]; therefore it confirms the magnetic-field induced effect that is presented in the paper.

Next, we would like to elucidate the origin of the dip at 185 cm^{-1}. Supplementary Fig. 5(a) and (b) shows the c-axis reflectivity and the real part of the conductivity of the Y-123 sample with $T_\mathrm{c} = 58$ K (the one presented in Fig. 3. of the paper) on a magnified scale. It is clear, that the relatively weak phonon structure in the range of 185-195 cm^{-1} exhibits very large and anomalous changes with temperature. This is due to the fact, that the phonon eigenvector involves a sizeable displacement of Yttrium ions [6] and that the intra-bilayer local fields are strongly modified by the depolarization charge density dynamically accumulated at the CuO_2 planes. Results of a simulation of the behaviour of a phonon corresponding to a vibration of intra-bilayer atom are given in Fig. 4(c) of Ref. [5]. It shows that the phonon lineshape exhibits a large softening upon entering the SC state, just as observed for the Y-mode in our present sample. Consequently, one can expect that this mode should exhibit fairly large magnetic-field induced changes.

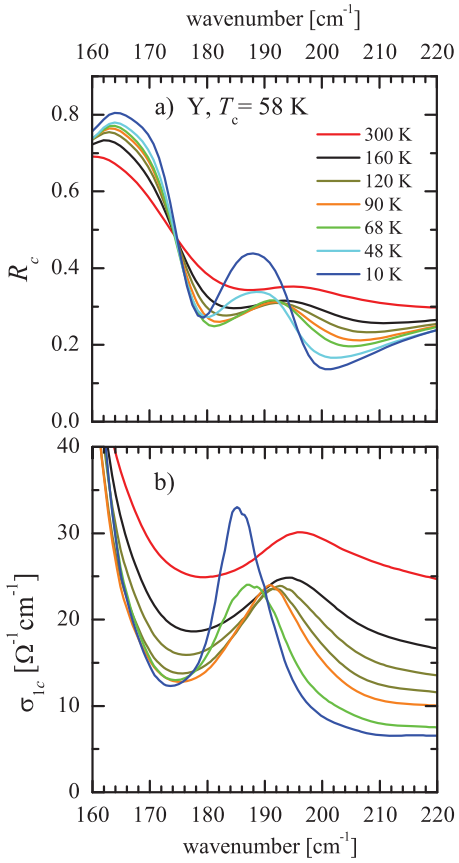

Fig. S 5: Spectra of the c-axis reflectivity (**a**), and the optical conductivity (**b**), showing the anomalous temperature dependence of the 185 cm^{-1} phonon for strongly underdoped Y-123 with T_c=58 K.

In the paper, it is discussed that the field induced effects at $T_\mathrm{c} < T < T^\mathrm{ons}$ are fairly small since the phase is strongly disordered already in the absence of the field and the field can be expected to have only a minor effect on the extent of the disorder. It is therefore essential that the measurements have a sufficient signal to noise. The signal to noise issue may be the reason why it was concluded that the magnetic field effects fade away within 20 K above T_c based on the microwave conductivity data [25] which were measured on some of the same Y-123 crystals with a lower signal to noise ratio of about 10^{-2} as compared to about 10^{-3} in our experiment. We note that field induced changes in a field of only 1 T observed in transport measurements with excellent signal to noise persists up to very high temperatures [26].

III. SIGNATURES OF THE PRECURSOR SUPERCONDUCTING STATE IN THE a-AXIS RESPONSE

In this paragraph we show that the temperature- and frequency dependence of the a-axis response of the underdoped Y-123 crystals is consistent with the scenario of a precursor superconducting state below $T^{\rm ons}$. In particular, the a-axis conductivity is found to undergo very similar spectral changes as the intra-bilayer conductivity $\sigma_{\rm bl}$ discussed in the paper.

In the infrared range it is well known that the in-plane conductivity exhibits a dip-like feature with a minimum around 400-500 cm^{-1} [27–32]. This feature is well known to be directly related to superconductivity since it becomes most pronounced below $T_{\rm c}$. It is furthermore well explained in terms of a Holstein-model of Bogoliubov-quasiparticles that are strongly coupled to a bosonic mode (phonons or spin fluctuations) [33, 34]. A weak dip feature was even previously shown to persist above $T_{\rm c}$, but its temperature dependence was not accurately determined [28, 31, 32]. In the following we show that this dip feature develops indeed at $T^{\rm ons}$ and that it gives rise to a downward shift of the spectral weight, similar as it is reported in the paper for the local conductivity within the bilayer unit, $\sigma_{\rm bl}$.

Supplementary Fig. 6 displays our spectra of σ_{1a} for a strongly underdoped Y-123 crystal with $T_{\rm c}$=61(2) K and $T^* > 300$ K. They confirm that a dip with a minimum around 400 cm^{-1} develops already well above $T_{\rm c}$. The inset of supplementary Fig. 6 details its temperature dependence in terms of the spectral weight between 250 and 1500 cm^{-1}. Its decrease below about $T^{\rm ons} \approx 160$ K confirms that the dip in σ_{1a} develops concurrently with the TPM and the phonon anomalies in the c-axis response [see Fig. 1(f) of the paper]. Our data also show that the missing spectral weight due to the dip formation is transferred to lower frequency, as expected for a PSC. In agreement with a previous report [29], we observe no significant increase of σ_{1a} above 1500 cm^{-1}.

The increase of the low-frequency weight below 160 K is confirmed by the temperature dependence of the real part of the dielectric function, ϵ_{1a}. Supplementary Fig. 7(a) shows ϵ_{1a}(125 cm^{-1}) whose decrease (towards larger negative values) with decreasing temperature reflects the increase of the spectral weight at frequencies below 125 cm^{-1}. Its gradual decrease towards larger negative values above 160 K is due to the well known narrowing of the very long Drude tail which occurs as well in optimally doped samples [30, 35]. The increased slope below $T^{\rm ons} = 160$ K confirms that the dip-feature gives rise to a faster increase of the spectral weight below 125 cm^{-1}.

Furthermore, supplementary Fig. 7(b) shows the temperature evolution of ϵ_{1a} above the gap, at 1500 cm^{-1}. Between 300 and 200 K, ϵ_{1a} also exhibits the gradual decrease due to the narrowing of the long tail of the Drude response. However, this trend is interrupted around

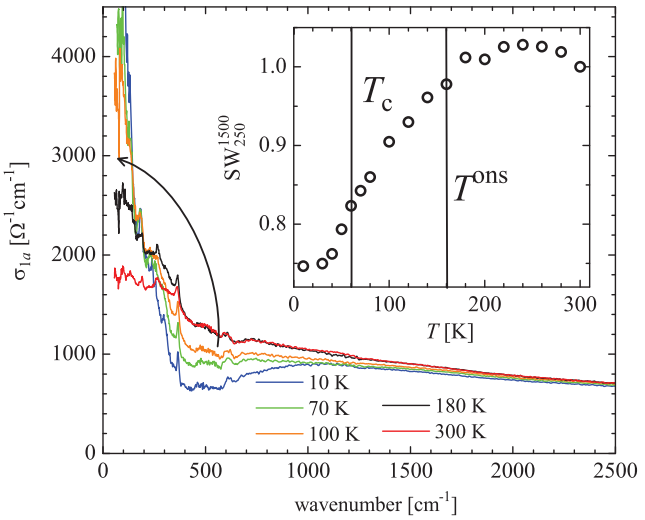

Fig. S 6: Real part of the a-axis infrared conductivity, σ_{1a}, of a detwinned Y-123 crystal that is underdoped with $T_{\rm c} = 61$ K. The arrow indicates the shift of spectral weight towards low frequency due to the dip feature around 500 cm^{-1} and the enhanced Drude-like response. The inset details the temperature dependence of the spectral weight (SW_{250}^{1500}) in the dip-region between 250 and 1500 cm^{-1} normalized to 300 K (circles) which starts to decrease below $T^{\rm ons} \approx 160$ K due to the formation of the dip-feature.

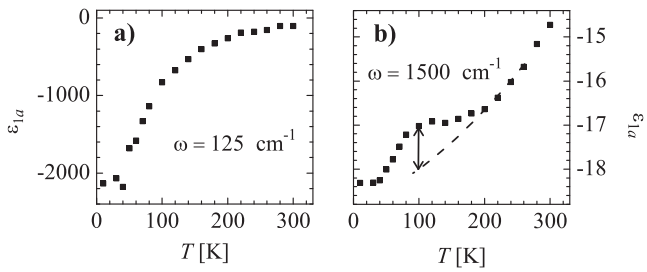

Fig. S 7: Temperature dependence of the real part of the dielectric function along the a-axis of the $T_{\rm c}$=61 K sample at 125 cm^{-1} **(a)** and above the gap at 1500 cm^{-1} **(b)**.

160 K where the decrease slows down and is partially compensated by a positive contribution to ϵ_{1a}. As shown in supplementary Fig. 8, this feature is a Kramers-Kronig counterpart of the dip-formation in σ_{1a} and the related spectral weight shift to lower frequencies. Supplementary Fig. 8(a) shows the experimental σ_{1a} at 180 K and 80 K, i.e. right above $T^{\rm ons} \approx 160$ K and $T_{\rm c}$=61 K, respectively. As shown in supplementary Fig. 8(b) we have approximated the dip-feature in σ_{1a} and the downward shift of the spectral weight (with a conserved total spectral weight) with triangular functions. Supplementary Fig. 8(c) shows ϵ_{1a} as computed from σ_{1a} of supplementary Fig. 8(b) by using the Kramers-Kronig relationship. Additionally to the pronounced decrease of ϵ_1 at low frequencies, the "80 K" spectrum exhibits an overshoot

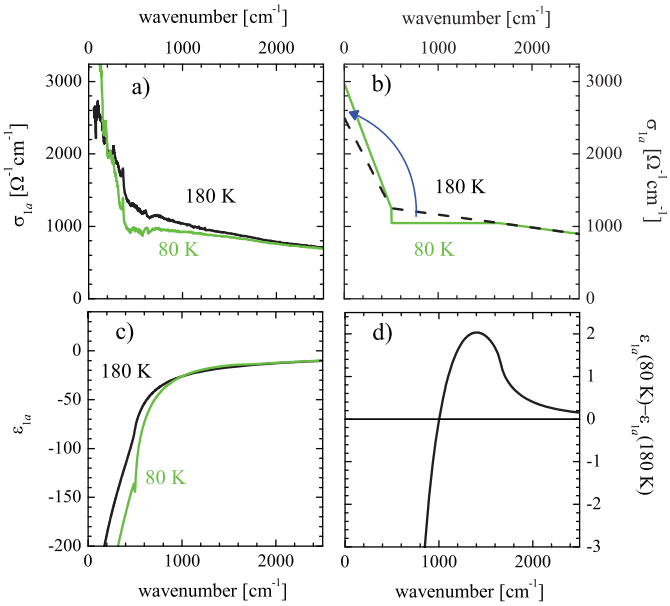

Fig. S 8: Experimental data (**a**) and simulation with triangular profiles **(b)** for the formation of the dip-feature due to the precursor superconducting gap in the a-axis response of a strongly underdoped Y-123 crystal with T_c=61 K. **c**, The real part of the dielectric function calculated via Kramers-Kronig transformation of the spectra in (b). **d**, The difference of the spectra shown in (c).

above the one at "180 K" at about 1500 cm^{-1}, which is better seen in the difference $\epsilon_{1a}(80\ K) - \epsilon_{1a}(180\ K)$ as shown in supplementary Fig. 8(d). This overshoot is a consequence of the gap formation because the theoretical spectra of σ_{1a} [supplementary Fig. 8(b)] are identical above 1500 cm^{-1}. This overshoot is the reason of the upward trend seen in the supplementary Fig. 7(b). Note that the magnitude of this feature compares rather well to the experiment one (especially given the crudeness of our approximation): the maximum of the simulated overshoot is 2 [see supplementary Fig. 8(d)] and the magnitude of the wave in the experimental ϵ_{1a} measured from the extrapolated trend from 200-300 K is about 1 [see supplementary Fig. 7(b)].

We note that previous sub-THz spectroscopy measurements of the in-plane response of $Bi_2Sr_2CaCu_2O_{8+\delta}$ [36] resolved the SC fluctuations only at considerably lower temperatures. The difference between the sub-THz study and our analysis may be related to the difference in the probed frequency range since in our case we employ the TPM at 400-450 cm^{-1} (12-13 THz) in the c-axis response and the gap feature at about 400 cm^{-1} in the a-axis conductivity. For example, the fluctuating SC state can be spatially inhomogeneous, i.e., it can be formed by fluctuating SC domains in a normal state matrix. The effective response of such medium will not exhibit the delta function but the Drude term with finite broadening. However the effective response will exhibit the gap feature weakened proportionally to the ratio of the volume of the SC and normal state.

[1] Humlíček, J. Henn, R. Cardona, M. Infrared vibrations in $LaSrGaO_4$ and $LaSrAlO_4$. Phys. Rev. B **61**, 14554-14563 (2000).

[2] van der Marel, D. and Tsvetkov, A. Transverse optical plasmons in layered superconductors. Czechoslovak Journal of Physics **46**, 3165-3168 (1996).

[3] Grüninger, M. van der Marel, D., Tsvetkov, A. A. and Erb, A. Observation of out-of-phase bilayer plasmons in $YBa_2Cu_3O_{7-\delta}$. Phys. Rev. Lett. **84**, 1575-1578 (2000).

[4] Munzar, D. Bernhard, C. Golnik, A. Humlíček, J. and Cardona, M. Anomalies of the infrared-active phonons in underdoped $YBa_2Cu_3O_y$ as evidence for the intra-bilayer Josephson effect. Sol. Stat. Comm. **112**, 365-369 (1999).

[5] Dubroka, A. and Munzar, D. Phonon anomalies in trilayer high-T_c cuprate superconductors. Physica C **405**, 133-147 (2004).

[6] Henn, R. Strach, T. Schönherr, E. and Cardona, M. Isotope effects on the optical phonons of $YBa_2Cu_3O_7$: Eigenvector and infrared charge determination. Phys. Rev. B **55**, 3285-3296 (1997).

[7] Wang, Y. Li Lu and Ong, N. P. Nernst effect in high-T-c superconductors Phys. Rev. B **73**, 024510 (2006).

[8] Meingast, C. *et al.* Phase fluctuations and the pseudogap in $YBa_2Cu_3O_x$. Phys. Rev. Lett. **86**, 1606-1609 (2001).

[9] Tallon, J.L. and Loram, J. W. The doping dependence of T^* - what is the real high-T-c phase diagram? Physica C **349**, 53-68 (2001).

[10] Tallon, J.L. Storey, J.G. and Loram, J.W. Fluctuations and Tc reduction in cuprate superconductors, arXiv0908.4428v1.

[11] Hinkov, V. *et al.* Spin dynamics in the pseudogap state of a high-temperature superconductor. Nat. Phys. **3**, 780-785 (2007).

[12] Hinkov, V. *et al.* Electronic Liquid Crystal State in the High-Temperature Superconductor $YBa_2Cu_3O_{6.45}$. Science **319**, 597-600 (2008).

[13] Andersen, O.K. Liechtenstein, A. I. Jepsen, O. and Paulsen, F. J. LDA energy bands, low-energy Hamiltonians, t', t'', $t_\perp(k)$, and $J_\perp$. Phys. Chem. Solids **56**, 1573-1591 (1995).

[14] Borisenko, S. V. *et al.* Kinks, nodal bilayer splitting, and interband scattering in $YBa_2Cu_3O_{6+x}$. Phys. Rev. Lett. **96**, 117004 (2006).

[15] Zabolotnyy, V. B. et al., Momentum and temperature dependence of renormalization effects in the high-temperature superconductor $YBa_2Cu_3O_{7-\delta}$. Phys. Rev. B **76**, 064519 (2007).

[16] Hirschfeld, P. J. Quinlan, S. M. Scalapino, D. J. c-axis infrared conductivity of a d(x2-y2)-wave superconductor with impurity and spin-fluctuation scattering Phys. Rev. B **55**, 12742 (1997).

[17] Shah, N. and Millis, A. J. Application of the scattering-

rate sum rule to the interplane optical conductivity of high-temperature superconductors: Pseudogap and bilayer effects. Phys. Rev. B **65**, 024506 (2001).

[18] Bernhard, C. *et al.* Far-infrared ellipsometric study of the spectral gap in the *c*-axis conductivity of $Y_{1-x}Ca_xBa_2Cu_3O_{7-\delta}$ crystals. Phys. Rev. B **59**, R6631-R6634 (1999).

[19] Tanaka, K. *et al.* Distinct Fermi-momentum-dependent energy gaps in deeply underdoped Bi2212. Science **314**, 1910-1913 (2006).

[20] Bernhard, C. *et al.* Anomaly of oxygen bond-bending mode at $320\,\mathrm{cm}^{-1}$ and additional absorption peak in the *c*-axis infrared conductivity of underdoped $YBa_2Cu_3O_{7-\delta}$ single crystals revisited with ellipsometric measurements. Phys. Rev. B **61**, 618 (2000).

[21] Chaloupka, J. and Munzar, D. Microscopic gauge-invariant theory of the *c*-axis infrared response of bilayer cuprate superconductors and the origin of the superconductivity-induced absorption bands. Phys. Rev. B **79**, 184513 (2009).

[22] Yu Li *et al.* Evidence for two separate energy gaps in underdoped high-temperature cuprate superconductors from broadband infrared ellipsometry. Phys. Rev. Lett. **100**, 177004 (2008).

[23] Hossain, M. A. *et al.* In situ doping control of the surface of high-temperature superconductors. Nature Physics **4**, 527-531 (2008).

[24] D. Fournier, *et al.* Loss of nodal quasiparticle integrity in underdoped $YBa_2Cu_3O_{7-\delta}$. Nature Phys. **6**, 905 (2010).

[25] Grbic, M. S. *et al.*, to be published, cond-mat arXiv:1005.4789 (2010).

[26] Ando, Y. and Segawa, K. Magnetoresistance of untwinned $YBa_2Cu_3O_y$ single crystals in a wide range of doping: anomalous hole-doping dependence of the coherence length. Phys. Rev. Lett. **88**, 167005 (2002).

[27] Timusk, T. and Statt, B. The pseudogap in high-temperature superconductors: an experimental survey. Rep. Prog. Phys. **62**, 61 (1999).

[28] Basov, D. N. and Timusk, T. Electrodynamics of high Tc superconductors. Rev. Mod. Phys. 77, 721 (2005).

[29] Santander-Syro, A. F. *et al.* Absence of a loss of in-plane infrared spectral weight in the pseudogap regime of $Bi_2Sr_2CaCu_2O_{8+\delta}$. Phys. Rev. Lett. **88**, 097005 (2002).

[30] Boris, A. V. *et al.* In-plane spectral weight shift of charge carriers in $YBa_2Cu_3O_{6.9}$. Science **304**, 708-710 (2004).

[31] Hwang, J. Timusk, T. and Gu, G. D. Doping dependent optical properties of $Bi_2Sr_2CaCu_2O_{8+\delta}$. J. Phys.: Condens. Matter **19**, 125208 (2007).

[32] Hwang, J. Yang, J. Carbotte, J.P. and Timusk, T. Manifestation of the pseudogap in *ab*-plane optical characteristics. J. Phys.: Condens. Matter **20**, 295215 (2008).

[33] Munzar, D. Bernhard, C. Cardona, M. Does the peak in the magnetic susceptibility determine the in-plane infrared conductivity of YBCO? Physica C **312**, 121-135 (1999).

[34] Carbotte, J.P. Schachinger, E. and Basov, D.N. Coupling strength of charge carriers to spin fluctuations in high-temperature superconductors. Nature **401**, 354-356 (1999).

[35] Ortolani, M. Calvani, P. and Lupi, S. Frequency-dependent thermal response of the charge system and the restricted sum rules of $La_{2-x}Sr_xCuO_4$. Phys. Rev. Lett. **94**, 067002 (2005).

[36] Corson, J. Mallozzi, R. Orenstein, J. Eckstein, J. N. and Bozovic, I. Vanishing of phase coherence in underdoped $Bi_2Sr_2CaCu_2O_{8+\delta}$. Nature **398**, 221-223 (1999).